

Reimagining Target-Aware Molecular Generation through Retrieval-Enhanced Aligned Diffusion

Dong Xu^{1,2} Zhangfan Yang³ Ka-Chun Wong⁴ Zexuan Zhu^{1,2} Jianqiang Li^{1,2} Junkai Ji^{1,2*}

¹ School of Artificial Intelligence, Shenzhen University

² National Engineering Laboratory for Big Data System Computing Technology, Shenzhen University

³ School of Computer Science, University of Nottingham Ningbo

⁴ Department of Computing, The Hong Kong Polytechnic University

Abstract

Breakthroughs in high-accuracy protein structure prediction, such as AlphaFold, have established receptor-based molecule design as a critical driver for rapid early-phase drug discovery. However, most approaches still struggle to balance pocket-specific geometric fit with strict valence and synthetic constraints. To resolve this trade-off, a Retrieval-Enhanced Aligned Diffusion termed READ is introduced, which is the first to merge molecular Retrieval-Augmented Generation with an SE(3)-equivariant diffusion model. Specifically, a contrastively pre-trained encoder aligns atom-level representations during training, then retrieves graph embeddings of pocket-matched scaffolds to guide each reverse-diffusion step at inference. This single mechanism can inject real-world chemical priors exactly where needed, producing valid, diverse, and shape-complementary ligands. Experimental results demonstrate that READ can achieve very competitive performance in CBGBench, surpassing state-of-the-art generative models and even native ligands. That suggests retrieval and diffusion can be co-optimized for faster, more reliable structure-based drug design.

1 INTRODUCTION

The convergence of high-resolution structural biology and generative AI has ushered in a new era of rational drug design. Breakthroughs in cryo-EM and geometric deep learning now permit direct generation of ligand molecules within three-dimensional protein pockets, effectively unifying structural insight with chemical synthesis [1, 2, 3, 4]. Yet state-of-the-art generators still face a fundamental conflict: they must be stochastic enough to explore chemical space while simultaneously obeying the rigid geometric and energetic laws to govern molecular interactions.

Limitations of autoregressive frameworks. Early structure-conditioned methods such as Pocket2Mol [5] and GraphBP [8] assemble molecules in an atom-by-atom autoregressive manner. The resulting sequential bias accumulates errors and often traps the search in local optima [6]. Furthermore, their Cartesian-coordinate parametrization lacks rotational equivariance, leading to steric clashes [7]. Remedies based on multi-scale modelling [10] or fragment-level constraints [11] alleviate some artifacts but introduce substantial architectural and training complexity.

Promise and pitfalls of diffusion models. Generators based on diffusion recast molecule synthesis as a step-by-step denoising process [12, 13, 14, 16, 17]. Equivariant variants [18, 19, 25] deliver markedly improved spatial fidelity, whereas the methods that pioneer *target-aware* diffusion-based ligand generation explicitly condition the denoising process on pocket information [22, 26]. Neverthe-

*Corresponding author: jijunkai@szu.edu.cn

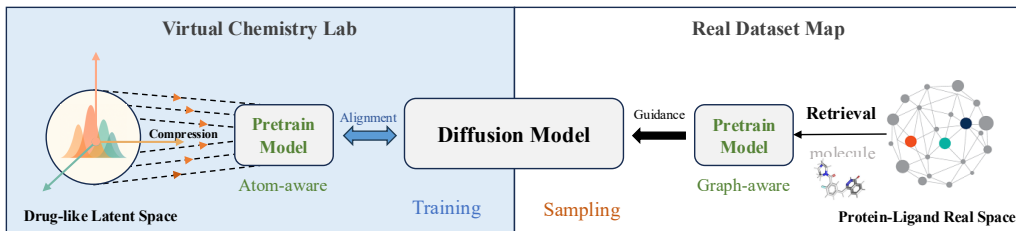


Figure 1: READ overview. The diffusion model aligns atom-level representations with those of a pre-trained encoder, operating within a drug-like latent manifold. During sampling, template molecules retrieved from a pocket-similarity graph supply pre-trained embeddings that steer the denoising trajectory toward synthetically accessible, pocket-compatible ligands.

less, the injected uniform Gaussian noise can not align with the geometry of chemical bonds and often leads to invalid valence states or distorted three-dimensional conformations [41]. Corrections applied *post hoc*, such as the evolutionary optimization used in DiffSBDD [20] or the integrated scheme implemented in UniMoMo, mitigate these artifacts yet do not entirely eliminate the underlying mismatch [29].

Retrieval-Enhanced Aligned Diffusion (READ). To address the above issues, a Retrieval-Enhanced Aligned Diffusion (READ) model is proposed, which fuses latent diffusion with empirical chemical knowledge in the two phases of molecular generation, as illustrated in Fig. 1. In the first phase, a three-dimensional latent manifold is learned from six million MMFF-optimised [30] ZINC molecules via contrastive learning that combines random coordinate perturbations with atom masking [42]. This encoder embeds physicochemical metrics and geometric constraints directly into latent gradients, eliminating handcrafted validity filters. In the second phase, a protein-pocket index built with TM-align [32] and DaliLite [33] retrieves ligand templates via coarse structural matching followed by local neighbor refinement [23]. Their pre-trained embeddings modulate the diffusion steps through a cross-modal alignment module, balancing exploration with pocket-specific exploitation. To our knowledge, READ is the first retrieval-augmented diffusion framework for *de novo* ligand design.

The contributions of this study can be summarized as follows:

- We demonstrate that contrastive pretraining alone suffices to encode chemical validity into latent topology and obviate handcrafted constraints.
- We introduce a hierarchical retrieval strategy that jointly optimizes exploration and exploitation via context-aware guidance.
- By tightly coupling latent diffusion with empirical knowledge, READ establishes a principled path toward synthesizable and target-specific molecule generation.

2 Related Work

Structure-Based Drug Design. Structure-based molecular generation has advanced from sequential coordinate prediction to three-dimensional geometric reasoning. Early autoregressive generators broke rotational symmetry and imposed sequential biases [5, 6, 8]. Subsequent schemes that fuse multi-scale features [10] or enforce fragment-based restraints [11] improved chemical validity, but increased architectural complexity and reduced training stability. More recent diffusion-based approaches capture long-range interactions through iterative denoising. For instance, EDM [18] introduced equivariant diffusion, GeoLDM [25] leveraged a geometric latent space to boost sampling efficiency, and TargetDiff [22] refined local coordinate projections for enhanced binding specificity. Nonetheless, Gaussian perturbations inherent to these methods still distort bond lengths and angles [41], resulting in valence errors and warped conformers [27]. Attempts to incorporate fragment priors via stitching, such as FLAG [28] and DrugGPS [34], mitigate some issues yet introduce unnatural linkage patterns. AlignDiff [21] leverages preference optimization to post-training a pretrained diffusion model.

Retrieval-Augmented Generation. Retrieval-augmented generation (RAG) enriches generative models by integrating exemplar data from large repositories [35]. Originating with the Retrieve-and-Read

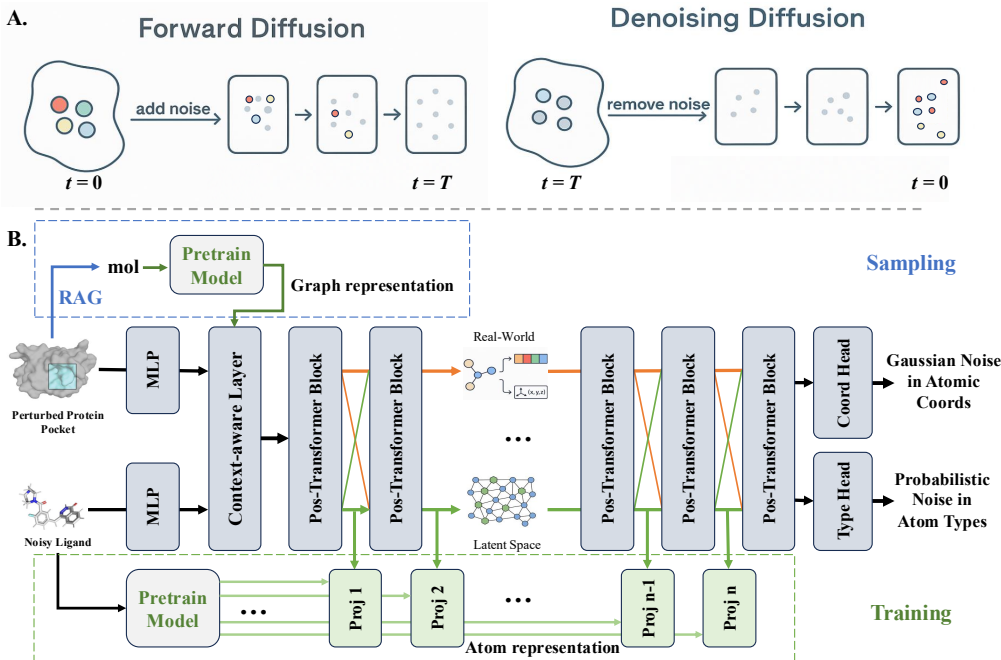


Figure 2: READ pipeline. (A) Forward diffusion injects Gaussian noise into atomic coordinates and categorical noise into atom types, while the reverse process iteratively removes noise to recover a valid ligand and its position. (B) At inference, a context-aware encoder fuses a perturbed pocket-ligand pair with graph embeddings of template molecules retrieved by RAG from the pretrained latent manifold, steering the coordinate and type heads during denoising. The green branch (bottom) is used only in training to align diffusion states with the latent space via multi-layer projections and is omitted at sampling time.

paradigm, it evolved into end-to-end differentiable frameworks such as DRAGON [37] and GraphRAG’s structured retrieval over molecular interaction graphs [36]. In drug design, some methods retrieve whole molecules or fragments to guide assembly: DeLinker [38] selects linkers from fragment libraries; RetMol [53] fuses exemplar compounds to steer generation toward target properties; and f-RAG [39] injects relevant fragments to balance diversity and validity. Others project retrieved molecules into pre-trained latent spaces to inform diffusion trajectories, as demonstrated by MolR[40]. However, fragment stitching can cause substructure mismatches, and global latent retrieval may introduce irrelevant features. Our hierarchical cross-modal retrieval mechanism overcomes these limitations by adjusting retrieval granularity and aligning geometric features across modalities.

3 Methodology

3.1 Generative Framework with Latent-Aligned Diffusion

The READ formulated the pocket-conditioned ligand generation as a retrieval-augmented diffusion process operating in two interleaved spaces: the molecular structure space $\mathcal{M} = (\mathbf{X}, \mathbf{V})$, where $\mathbf{X} \in \mathbb{R}^{N \times 3}$ denotes atomic coordinates and $\mathbf{V} \in \{0, 1\}^{N \times K}$ atom types; and the latent chemical space \mathcal{Z}_m pre-trained to encode physicochemical constraints. Given a protein pocket $\mathcal{P} = (\mathbf{X}_p, \mathbf{V}_p)$, our goal is to learn a conditional distribution $p_\theta(\mathcal{M}|\mathcal{P})$ that respects both geometric complementarity and synthetic feasibility.

The generation process integrates three components through stochastic differential equations:

$$d\mathcal{M}_t = \underbrace{f_\theta(\mathcal{M}_t, t|\mathcal{P})dt + g_t d\mathbf{w}}_{\text{Diffusion Dynamics}} + \underbrace{\lambda \cdot \mathbb{E}_{\mathcal{M}_k \sim \mathcal{Z}_r(\mathcal{P})}[\phi(\mathcal{M}_k)]}_{\text{Retrieval Guidance}}, \quad (1)$$

where f_θ parameterizes the equivariant denoiser, g_t controls noise scales, and $\phi(\cdot)$ projects retrieved ligands \mathcal{M}_k from the pre-trained space \mathcal{Z}_m into diffusion trajectories. The retrieval space \mathcal{Z}_r is constructed as a graph with nodes $\{\mathcal{P}_i, \mathcal{M}_i\}$ and edges weighted by structural similarity metrics.

Diffusion in Dual Spaces Our framework orchestrates simultaneous diffusion in molecular coordinates and atom types through coupled stochastic processes. For the 3D coordinates \mathbf{X} , a variance-exploding SDE is adopted to accelerate geometry relaxation [15, 22]:

$$q(\mathbf{X}_t|\mathbf{X}_0) = \mathcal{N}(\mathbf{X}_t; \mathbf{X}_0, \sigma_t^2 \mathbf{I}), \quad \sigma_t = \beta_{\max} \cdot t^2 + \beta_{\min}, \quad (2)$$

where the quadratic variance schedule enables rapid exploration of conformational space while preserving geometric continuity through equivariant graph convolutions. Atom types \mathbf{V} follow an absorbing-state diffusion process that maintains chemical validity:

$$q(\mathbf{V}_t|\mathbf{V}_{t-1}) = \alpha_t \mathbf{V}_{t-1} + (1 - \alpha_t) \mathbf{U}_K, \quad \mathbf{U}_K \sim \text{Uniform}\{1, \dots, K\}, \quad (3)$$

where the learned transition matrix \mathbf{U}_K enforces type consistency by only allowing transitions to valid atom types. The joint reverse process integrates both modalities through cross-modal attention:

$$p_\theta(\mathbf{X}_{t-1}, \mathbf{V}_{t-1}|\mathbf{X}_t, \mathbf{V}_t, \mathcal{P}) = \mathcal{N}(\mathbf{X}_{t-1}; \mu_\theta(\mathbf{X}_t, \mathbf{h}_t), \Sigma_t) \cdot \text{Cat}(\mathbf{V}_{t-1}; \pi_\theta(\mathbf{h}_t)), \quad (4)$$

where the latent state $\mathbf{h}_t = \text{EGNN}(\mathbf{X}_t, \mathbf{V}_t) + \text{Attn}(\mathbf{X}_t, \phi(\mathcal{M}_k))$ combines local structural reasoning from EGNN [44] with global prior knowledge retrieved from pretrained latent space \mathcal{Z}_m . This dual-path design inherently addresses geometric and chemical constraints through coupled stochastic processes. Variance-controlled diffusion can guide \mathbf{X} -space exploration and absorb probabilities in \mathbf{V}_t enforce type consistency, by cross-modal attention mediating between local optimization and global prior knowledge.

3.2 Latent Space Pretraining for Alignment

A hierarchical pretraining–synthesis framework is introduced to learn a unified latent space \mathcal{Z}_m spanning atomic, geometric, and diffusion-step representations. Each atom a_i is mapped to an eight-dimensional vector that fuses 3-D coordinates with key chemical descriptors—atom type, chirality, aromaticity, hybridization, and related attributes. Categorical attributes are embedded with learnable dictionaries $\mathbf{D}_k \in \mathbb{R}^{d_k \times |C_k|}$, whereas continuous features remain in their original scale.

Corpora and augmentations. Starting from six million ZINC compounds that satisfy standard drug-likeness constraints, four complementary graph–geometry views are created for every molecule—atom masking, bond perturbation, subgraph removal, and small coordinate perturbations, thereby decoupling chemical validity from geometric stability [43].

Atom-aware contrastive objective. View pairs are encoded by an SE(3)-equivariant GNN and aligned with a temperature-scaled InfoNCE objective in Eq. (5), applied at multiple depths through layer-specific projectors. This multi-resolution alignment teaches the encoder to disentangle geometric consistency from synthetic accessibility without handcrafted rules.

$$\mathcal{L}_{\text{InfoNCE}} = -\log \frac{\exp(s(g, g^+)/\tau)}{\exp(s(g, g^+)/\tau) + \sum_{g^-} \exp(s(g, g^-)/\tau)}, \quad s(a, b) = \frac{a^\top b}{\|a\| \|b\|}, \quad (5)$$

where $s(a, b)$ denotes the cosine similarity; g^+ and g^- are the positive and negative masked-graph embeddings; g is the original (unmasked) graph embedding; and $\tau > 0$ is the temperature hyperparameter.

Representation Alignment for Graph Neural Network. During training, alignment is imposed layer-wise between the diffusion model’s hidden states and the pretrained ligand embeddings retrieved from the pocket–ligand database. Specifically, let $x_t = x + \epsilon \sqrt{\alpha_t}$ be the noisy input at timestep t , and let $h_\theta^{(l)}(x_t) \in \mathbb{R}^d$ denote the l -th layer hidden state of the diffusion model. For each retrieved ligand \mathcal{M}_k , pretrained model extract its embedding $y_{\phi,k}^{(l)} \in \mathbb{R}^d$ at the same layer l . The alignment loss is then defined as

$$\mathcal{L}_{\text{align}} = -\mathbb{E}_{\mathcal{M}, \epsilon, t} \left[\frac{1}{L} \sum_{l=1}^L \sum_{k=1}^K \log \frac{\exp(s(h_\theta^{(l)}(x_t), y_{\phi,k}^{(l)})/\tau)}{\sum_{j=1}^K \exp(s(h_\theta^{(l)}(x_t), y_{\phi,j}^{(l)})/\tau)} \right], \quad (6)$$

where $s(a, b) = a^\top b / (\|a\| \|b\|)$ is cosine similarity, K is the number of retrieved ligands, and $\tau > 0$ is the temperature. This mechanism ensures that, at each diffusion layer, the denoising trajectory is guided toward pockets-matched chemical priors, yielding conformations that are both energetically favorable and synthetically viable without explicit bond or valence constraints.

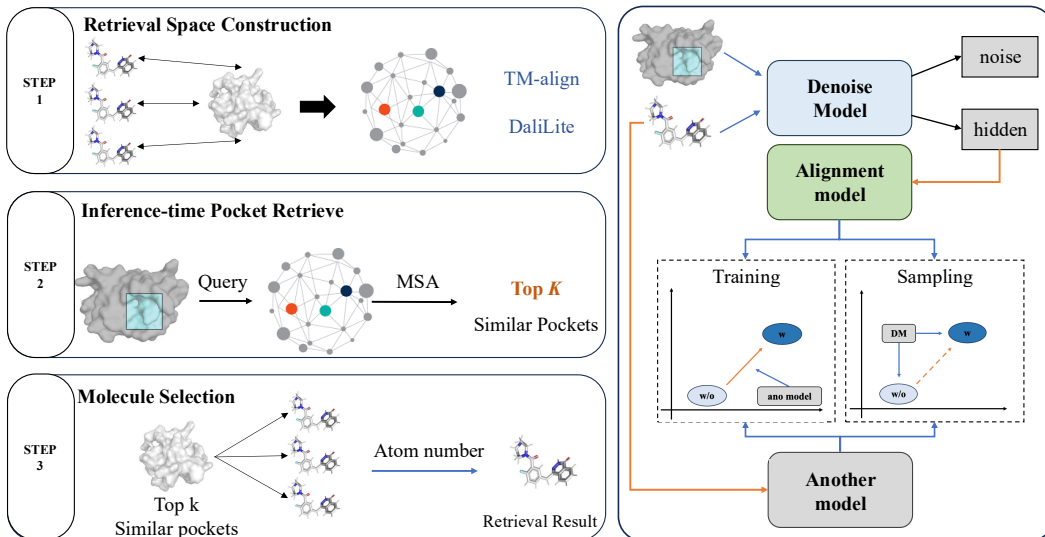


Figure 3: Workflow of the hierarchical retrieval augmented guidance. Hierarchical retrieval-augmented guidance pipeline: (Step 1) Construct a pocket–ligand graph by linking pockets to their cognate ligands and weighting pocket–pocket edges with averaged TM-Align and DaliLite scores; (Step 2) At inference, use MSA to align the query pocket to a set of distant seeds, then retrieve its top- K nearest neighbors; (Step 3) Select and embed ligands from those neighbors and fuse their embeddings into the denoiser. The right panel illustrates how an additional alignment model integrates retrieved embeddings via distinct strategies during training versus sampling.

3.3 Hierarchical Retrieval-Augmented Guidance

The retrieval module closes the feedback loop between prior chemical knowledge and the latent aligned diffusion dynamics in Sec. 3.1. The guidance term can be described by $\mathcal{G}(\mathcal{P}) = \lambda \mathbb{E}_{\mathcal{M}_k \sim \mathcal{Z}_r(\mathcal{P})} [\phi(\mathcal{M}_k)]$, where \mathcal{Z}_r is the pocket–ligand graph. The rest of this subsection describes how the graph is constructed, queried, and fused into the denoiser.

(i) Graph construction. Starting from the CBGBENCH [9] training split, a bipartite graph [36] is built, where pocket nodes $\{\mathcal{P}_i\}$ connect to their cognate ligand nodes $\{\mathcal{M}_i\}$. Edges between pockets carry structural–similarity weights:

$$\text{sim}(\mathcal{P}_i, \mathcal{P}_j) = \frac{\text{TM-Align}(\mathcal{P}_i, \mathcal{P}_j) + \text{DaliLite}(\mathcal{P}_i, \mathcal{P}_j)}{2}. \quad (7)$$

Ligands are excluded from edge construction; this mirrors the sampling stage, where only pocket geometry is available.

(ii) Hierarchical querying in sampling. Given a target pocket \mathcal{P} , we avoid an exhaustive $\mathcal{O}(|\mathcal{Z}_r|)$ search by a two-stage routine. First, ten pockets are precomputed and maximally distant from all others. A fast MSA [46] aligns \mathcal{P} against these candidates, and chooses the closest one \mathcal{P}_\star as the entry node. Second, the alignment is refined within the K nearest neighbours of \mathcal{P}_\star (default $K = 40$), producing a shortlist $\{\mathcal{P}_\star^{(j)}\}$ whose ligands are ranked by pocket–ligand complementarity. This coarse-to-fine pipeline reduces wall time by an order of magnitude while preserving the recall of biologically relevant templates.

(iii) Embedding and fusion. For the top m ligands (default $m = 4$), the pretrained embeddings $\phi(\mathcal{M}_k) \in \mathcal{Z}_m$ are obtained by the contrastive encoder from Sec. 3.2. At diffusion step t , the hidden state of the pre-trained model is updated by $\mathbf{h}_t \leftarrow \mathbf{h}_t + \text{Context-aware}(\mathbf{h}_t, \phi(\mathcal{M}_k))$, thereby realizing $\mathcal{G}(\mathcal{P})$ within the stochastic differential equation. Since one embedding set is reused along the reverse trajectory, the added cost can be negligible compared with force field post-processing.

(iv) Synergy with dual space noise. The denoiser alternates coordinate updates with feature updates. Retrieved ligand embeddings influence both streams: in the type noise branch, they bias the categorical logits of Eq. 3, steering atom type recovery toward privileged chemistries; in the geometry noise

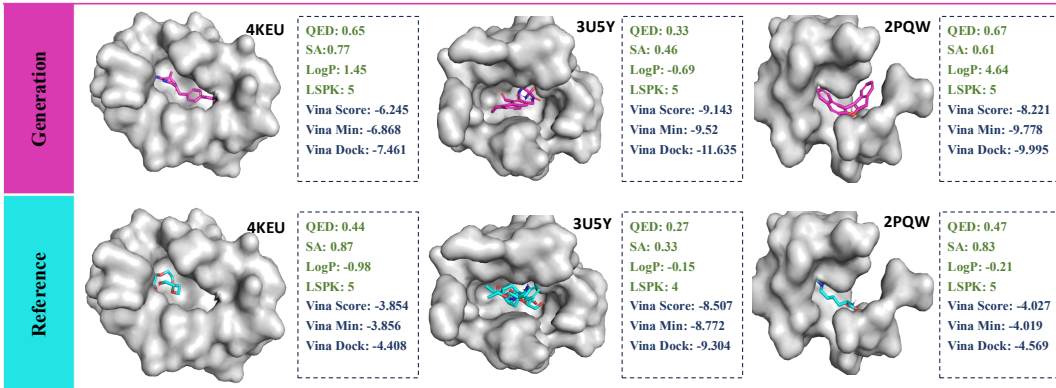


Figure 4: **Qualitative assessment of READ candidates.** For three representative CBGBench targets—4KEU, 3U5Y and 2PQW (columns, left to right)—the top row displays the best READ ligand selected from 100 samples while the bottom row shows the crystallographic reference ligand. The pocket surface is rendered in grey to highlight shape complementarity. Dash-outlined panels list drug-likeness metrics (QED, SA, $\log P$ and Lipinski heavy-rule count, LSPK) together with the three AutoDock-Vina energies reported throughout the paper: *Score*, *Minimize* and *Dock*. Across all pockets the READ molecules exhibit markedly lower (better) Vina energies than their native counterparts—often by more than 2 kcal mol⁻¹—while preserving acceptable synthetic accessibility and physicochemical profiles, visually confirming the quantitative gains reported in Sec. 4

branch, they act as attractors in Eq. 2, pulling Gaussian point clouds toward known pharmacophoric motifs. This coupling reconciles global pocket similarity with local stereochemistry, succeeding where purely stochastic diffusion often fails.

4 Experiment

The proposed READ is evaluated on **CBGBench** [9]. For each protein pocket, the READ generates one hundred candidate ligands, discarding those with positive Vina energy (larger than 0 kcal/mol), valence errors, or severe steric clashes. AutoDock Vina [47] is run in the Score, Minimize and Dock modes, yielding the mean Vina energy $E_{\text{Vina}} \downarrow$ and the improvement rate over reference ligands IMP \uparrow . Dock mode additionally reports the mean percentage binding gap MPBG \uparrow and ligand-binding efficacy LBE \uparrow , both normalized for molecular size. Interaction-pattern fidelity is quantified with PLIP v3.2 [52]: Jensen-Shannon divergence JSD \downarrow and mean absolute error MAE \downarrow are computed across seven interaction classes at the per-pocket and global levels. Here, \uparrow indicates higher-is-better whereas \downarrow indicates lower-is-better. Our approach is compared with twelve leading baselines: *autoregressive* generators (Pocket2Mol [5], GraphBP [8], 3DSBDD [49]); *diffusion* models (TargetDiff [22], DecompDiff [24], DiffBP [26], DiffSBDD [20]); *fragment* generators (FLAG [28], D3FG [27]); and *voxel grid* methods (VoxBind [51], MolCraft [50]). All models are tested on the same CBGBench splits with default Vina settings and PLIP v3.2.

Training protocol. Each model is trained on a single NVIDIA A6000 (48 GB) using a batch size of 8 and Adam with a learning rate of 10^{-3} . Training lasts for 500,000 iterations (about six days of wall clock time); convergence is typically reached after 350,000 iterations, well below the 2.5 million iterations often used by competitors. We release two READ variants with 1000 and 2000 denoising steps, each containing twelve million parameters and sharing identical hyperparameters.

Sampling cost. Generating one hundred ligands requires 18 min for the 1000-step model and 35 min for the 2000-step model. Without retrieval-based guidance, these times fall to 15 min and 30 min, respectively. The retrieval graph comprises 2,200 protein nodes and 166,000 ligand nodes yet adds negligible overhead at inference.

4.1 Interaction analysis

Thirteen metrics have been listed together with a Friedman weighted ranking in Table 1, where Dock-mode metrics double weight, and all others single weight. **READ-2k achieves Rank 1 overall,**

surpassing every baseline across the composite score. Although LiGAN retains the best raw Vina scores under Score and Minimize modes, READ-2k secures the strongest E_{Vina} and MPBG in the Dock mode by injecting pocket-matched scaffolds at every reverse-diffusion step. Relative to voxel-grid methods, READ reduces the global JSD_{OA} and MAE_{OA} , demonstrating finer atom-level contact fidelity. Compared with the best diffusion competitor, READ-2k shows the smallest PLIP divergences and errors, thus preserving pharmacophoric patterns most faithfully. It also records the highest validity rate and the top diffusion-only rank, confirming that contrastive pretraining together with retrieval guidance can balance binding affinity, interaction fidelity and chemical plausibility better than any other model.

Table 1: Comparison of various generation models on interaction analysis

Metric	Vina Score		Vina Min		Vina Dock				PLIP Interaction				Validity	Rank
	Evina	IMP	Evina	IMP	Evina	IMP	MPBG	LBE	JSD_{OA}	MAE_{OA}	JSD_{PP}	MAE_{PP}		
VoxBind [51]	-6.15	<u>41.80</u>	<u>-6.82</u>	<u>50.02</u>	-7.68	52.91	<u>9.89</u>	0.3588	0.0257	0.0533	0.1850	0.4606	0.74	<u>4.88</u>
MolCraft [50]	-6.15	54.25	-6.99	56.43	-7.79	56.22	8.38	0.3638	0.0214	0.0780	0.1868	0.4574	0.95	<u>5.29</u>
3DSBDD [49]	-	3.99	-3.75	17.98	-6.45	31.46	9.18	<u>0.3839</u>	0.0392	0.0934	0.1733	0.4231	0.54	7.29
GraphBP [8]	-	0.00	-	1.67	-4.57	10.86	-30.03	0.3200	0.0462	0.1625	0.2101	0.4835	0.66	10.18
Pocket2Mol [5]	-5.23	31.06	-6.03	38.04	-7.05	48.07	-0.17	0.4115	0.0319	0.2455	<u>0.1535</u>	0.4252	0.75	7.00
TargetDiff [22]	-5.71	38.21	-6.43	47.09	-7.41	51.99	5.38	0.3537	<u>0.0198</u>	0.0600	0.1757	0.4687	<u>0.96</u>	5.53
DiffBP [26]	-	8.60	-	19.68	-7.34	49.24	6.23	0.3481	0.0249	0.1430	0.1256	0.5639	0.78	6.76
DiffSBDD [20]	-	12.67	-2.15	22.24	-5.53	29.76	-23.51	0.2920	0.0333	0.1461	0.1777	0.5265	0.71	8.53
FLAG [28]	-	0.04	-	3.44	-3.65	11.78	-47.64	0.3319	0.0170	0.0277	0.2762	<u>0.3976</u>	0.68	8.47
D3FG [27]	-	3.70	-2.59	11.13	-6.78	28.90	-8.85	<u>0.4009</u>	0.0638	<u>0.0135</u>	0.1850	0.4641	0.77	8.12
DecompDiff [24]	-5.18	19.66	-6.04	34.84	-7.10	48.31	-1.59	0.3460	0.0215	0.0769	0.1848	0.4369	0.89	7.42
READ-1k	-5.32	34.75	-6.10	41.76	<u>-7.70</u>	<u>54.82</u>	<u>10.20</u>	0.3706	0.0276	0.0452	<u>0.1620</u>	<u>0.4216</u>	<u>0.97</u>	5.65
READ-2k	<u>-5.84</u>	<u>40.04</u>	<u>-6.20</u>	<u>47.10</u>	-7.79	<u>54.31</u>	12.33	0.3693	<u>0.0200</u>	0.0091	0.1644	0.3909	0.98	4.59

Per-pocket docking gains. Figure 5 provides a pocket-wise view of READ’s behaviour. Panels (a-c) plot the distribution of docking-score differences between the native ligand and the top candidate generated by READ under Score, Minimize, and Dock modes. Each histogram is strongly right-skewed, declines in performance are rare, and most pockets enjoy an apparent energy reduction. The grey bars mark the few pockets where the reference ligand remains superior, whereas the light-blue bars dominate the range of positive gains. This pattern shows that READ rarely sacrifices binding affinity in pursuit of novelty; it tends instead to return ligands that improve upon the crystal binder while still passing stringent drug-likeness filters. Panels (d-f) sharpen the view by scattering each pocket’s reference energy against the best READ energy, with color indicating the magnitude of the improvement. The cloud of points sits above the diagonal of parity for every protocol, and deeper shades congregate where the reference ligand is weakest. Hence, READ compensates precisely where conventional design struggles, yielding its largest gains on the most challenging pockets. We attribute this behavior to two factors. First, latent alignment embeds chemical priors that discourage invalid or over-strained conformations, so the energy landscape explored by the model excludes many of the traps that hinder earlier diffusion generators. Second, hierarchical retrieval supplies pocket-matched scaffolds that guide reverse diffusion toward regions of chemical space already validated by nature. Taken together with the aggregate results in Table 1, the figure confirms that READ’s **Rank 1** standing is not driven by a handful of favorable cases but reflects a consistent uplift across nearly all targets. The method raises the floor and ceiling, lifting weak binders into a therapeutically relevant energy range while further polishing already strong complexes.

4.2 Ablation study

Table 2 contrasts three configurations. Baseline employs a denoiser that has never seen the contrastive encoder, Baseline, RAG augments this unaligned model with retrieval, and READ integrates both alignment and retrieval in a single training loop. The comparison highlights two key observations. First, merely injecting one template embedding into an unaligned backbone yields only modest benefits, and coupling that same backbone with retrieval actually degrades the raw Vina score. A latent mismatch prevents the guidance signal from propagating into spatial coordinates. Second, aligning the denoiser to the encoder already lifts all interaction metrics, confirming that representation agreement regularises internal features. When retrieval is then activated on the aligned model, every

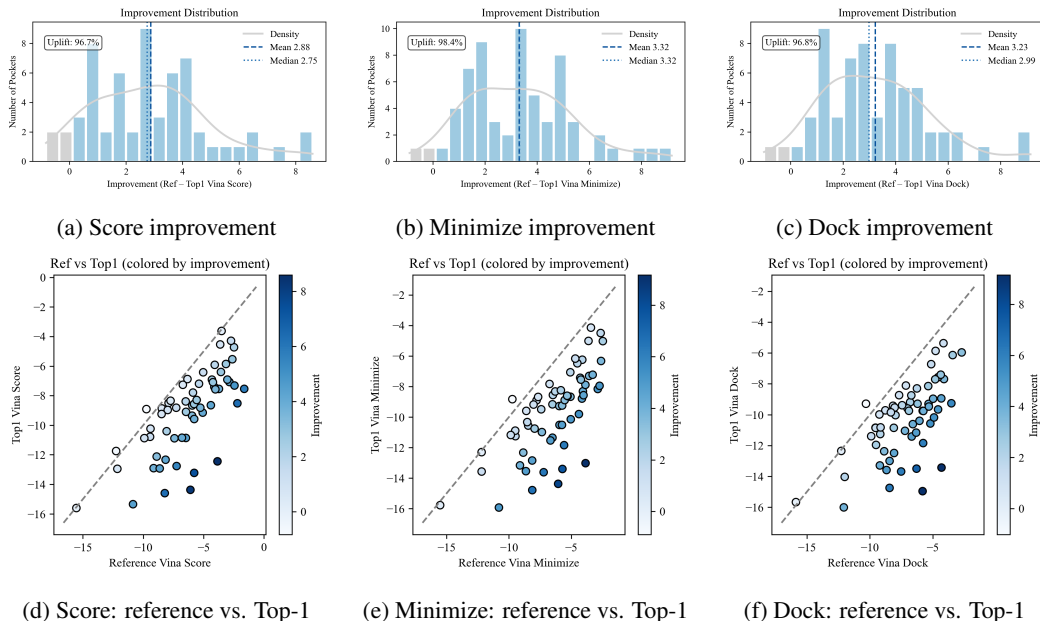


Figure 5: (a–c) Distribution of docking-performance gains achieved by selecting. For each protein pocket, the top-scoring ligand (of 100 generated) satisfies drug-likeness filters (QED > 0.5, SA > 0.6, Lipinski = 5) relative to the native ligand. Gray bars indicate cases where performance declined; light-blue bars indicate improvements. READ attains improvement probabilities of 96.7%, 98.4% and 96.8% for Score, Minimize and Dock, with mean Vina-score reductions of 2.88, 3.32 and 3.23, respectively. (d–f) Scatter plots of reference versus Top-1 docking metrics for Score, Minimize and Dock, colored by improvement magnitude. The dashed diagonal marks parity; the preponderance of points below it confirms that READ almost invariably generates drug-like molecules whose docking performance exceeds that of the native reference.

Table 2: Ablation analysis of interaction metrics

Method	Vina Score		Vina Min		Vina Dock			
	Evina	IMP	Evina	IMP	Evina	IMP	MPBG	LBE
Baseline w/o RAG	-5.72	33.91	-6.23	40.99	-7.10	43.44	5.13	0.3412
Baseline	-4.89 (-14.5%)	32.37 (-4.5%)	-6.29 (+1.0%)	42.81 (+4.4%)	-7.27 (+2.4%)	48.50 (+11.6%)	3.87 (-24.5%)	0.3729 (+9.3%)
READ-1k w/o RAG	-5.54	34.61	-6.02	39.06	-7.40	50.44	1.24	0.3564
READ-1k	-5.32 (-4.0%)	34.75 (+0.4%)	-6.10 (+1.3%)	41.76 (+7.0%)	-7.70 (+4.1%)	54.82 (+8.7%)	10.20 (+722.6%)	0.3706 (+4.0%)
READ-2k w/o RAG	-5.35	27.29	-5.90	36.60	-7.07	44.46	1.15	0.3577
READ-2k	-5.84 (+9.2%)	40.04 (+46.7%)	-6.20 (+5.1%)	47.10 (+28.7%)	-7.79 (+10.2%)	54.31 (+22.2%)	12.33 (+972.2%)	0.3693 (+3.2%)

score rises sharply: the binding gap indicator grows by more than sevenfold under the shorter schedule and approaches a tenfold gain under the longer schedule. In plain language, alignment prepares the latent space and retrieval, then steers generation toward pocket-specific optima. Their combination, therefore, secures the **Rank 1** position in the weighted benchmark while each component in isolation remains limited.

4.3 Chemical fidelity

Table 3 compares how well the generators preserve substructure statistics and avoid steric clashes. By contrast, our unaligned diffusion baseline drifts in composition and shows frequent clashes. Once the model is aligned (READ-1k), the divergences already shrink, and adding retrieval (READ-2k) tightens them further, driving functional-group errors down and halving clash ratios, all while keeping static-geometry scores on par with the best voxel baselines. Together, these results demonstrate that READ excels in docking performance and chemical realism. Latent alignment supplies a chemically aware manifold, retrieval injects pocket-matched priors, and their synergy yields ligands that fit, bind, and respect real-world chemistry without resorting to heavy post-generation fixes.

Table 3: Substructure fidelity and geometric-clash analysis.

Method	Atom type		Ring type		Functional group		Static Geometry		Clash	
	JSD	MAE	JSD	MAE	JSD	MAE	JSD _{BL}	JSD _{BA}	Ratio _{cca}	Ratio _{cm}
VoxBind [51]	0.0942	0.3564	0.2401	0.0301	0.1053	0.0761	0.2701	0.3771	0.0103	0.1890
MolCraft [50]	<u>0.0490</u>	0.3280	0.2469	0.0264	0.1196	0.0477	<u>0.2250</u>	0.2683	0.0264	0.2691
3DSBDD [49]	0.0860	0.8444	0.3188	0.2457	0.2682	0.0494	0.5024	0.3904	0.2482	0.8683
GraphBP [8]	0.1642	1.2266	0.5061	0.4382	0.6259	0.0705	0.5182	0.5645	0.8634	0.9974
Pocket2Mol [5]	0.0916	1.0497	0.3550	0.3545	0.2961	0.0622	0.5433	0.4922	0.0576	0.4499
TargetDiff [22]	0.0533	<u>0.2399</u>	<u>0.2345</u>	0.1559	0.2876	<u>0.0441</u>	0.2659	0.3769	0.0483	0.4920
DiffBP [26]	0.2591	1.5491	0.4531	0.4068	0.5345	<u>0.0670</u>	0.3453	0.4621	0.0449	0.4077
DiffSBDD [20]	0.0529	0.6316	0.3853	0.3437	0.5520	0.0710	0.3501	0.4588	0.1083	0.6578
FLAG [28]	0.1032	1.7665	0.2432	0.3370	0.3634	0.0666	0.4215	0.4324	0.6777	0.9769
D3FG [27]	0.0644	0.8154	<u>0.1869</u>	0.2204	0.2511	0.0516	0.3727	0.4700	0.2115	0.8571
DecompDiff [24]	0.0431	0.3197	0.2431	0.2006	0.1916	0.0318	<u>0.2576</u>	<u>0.3473</u>	0.0462	0.5248
Baseline w/o RAG	0.1546	0.6859	0.5074	0.4784	0.6358	0.0712	0.3256	0.4685	0.0374	0.4025
READ-1k	0.0491	<u>0.2096</u>	0.2512	0.2153	0.3246	0.0480	0.2885	0.4625	0.0483	0.4870
READ-2k	<u>0.0489</u>	0.1728	0.2563	0.2480	0.3166	0.0508	0.3371	0.5140	<u>0.0262</u>	0.3709
READ-2k-prior	0.0537	0.6269	0.0815	<u>0.0654</u>	0.2789	<u>0.0380</u>	0.2170	0.4433	<u>0.0255</u>	<u>0.3523</u>

Moreover, for structural and geometric evaluation, a prior-informed paradigm was adopted: retrieved molecules were decomposed via BRICS, and a fragment comprising at least five heavy atoms was randomly selected and held fixed (i.e., no diffusion noise was applied to its atoms). This strategy reduced the number of atoms requiring denoising and led to improved preservation of ring types and functional groups. Although the introduction of an entirely new fragment occasionally resulted in larger deviations in atomic types compared to the reference ligand, geometric stability was enhanced and steric clash rates were significantly lowered.

5 Discussion

Experiment results show that **READ-2k sets a new state of the art** for pocket-conditioned ligand generation. Table 1 reports that READ-2k obtains the strongest mean dock energy and the largest percentage binding gap in the entire benchmark, which places the model at **Rank 1**. A validity rate nearly twice that of the next best method confirms that retrieval guidance generates chemically sound ligands without trading away affinity. Figure 5 (a–c) further illustrates that READ-2k improves docking for almost every pocket and lowers the mean Vina energy by a noticeable margin, with similar trends in Score and Minimize modes.

Alignment and retrieval in combination. The ablation in Table 2 distinguishes three settings. A model trained without alignment serves as the Baseline; adding retrieval to this unaligned model yields Baseline RAG; finally, READ applies both alignment and retrieval. Alignment on its own lifts the improvement rate but leaves the binding gap nearly unchanged, whereas retrieval on an unaligned backbone even harms the raw Vina score. Only when the two components act together does the binding gap expand by roughly one order of magnitude, showing that alignment prepares the latent space and retrieval and steers generation toward the pocket optimum.

Interaction fidelity. PLIP analysis confirms that READ reproduces pharmacophoric features more accurately than every diffusion competitor. It records the smallest Jensen–Shannon divergence and the lowest mean absolute error, indicating superior recovery of hydrogen bonds, hydrophobic contacts, and salt bridges—interactions that govern activity and selectivity in downstream assays.

Chemical realism. Table 3 reveals that READ narrows divergences in atom, ring, and functional-group statistics while cutting clash ratios almost in half relative to the unaligned baseline. Static-geometry scores remain on par with heavily post-processed methods such as UniMoMo, yet READ achieves these qualities directly from the generator without expensive clean-up.

Limitations and outlook. Dependence on a pre-constructed retrieval graph of about two thousand pockets and one hundred and sixty-six thousand ligands can hinder performance on novel targets. Separating pretraining from diffusion simplifies optimization but still leaves a gap that a full end-to-end framework might close, provided that stability controls are in place. Cross-modal attention and retrieval look-ups also add a modest overhead in memory and computing. Future work will enlarge

the retrieval library with model-generated ligands, embed differentiable scoring into the diffusion objective, and handle receptor flexibility through ensemble-based retrieval.

6 Conclusion

A retrieval-enhanced diffusion framework named READ is introduced in this study, which unites contrastive latent pretraining with hierarchical template guidance to generate pocket-compatible ligands. READ achieves top-tier validity and docking performance on CBGBench while preserving interaction fidelity and substructure accuracy, all with faster convergence and competitive sampling efficiency. Our results highlight the power of latent alignment and retrieval synergy, suggesting broad applicability to other structure-based generative tasks and opening avenues for adaptive, end-to-end diffusion designs.

References

- [1] Jumper, J., Evans, R., Pritzel, A., Green, T., Figurnov, M., Ronneberger, O., Tunyasuvunakool, K., Bates, R., Židek, A., Potapenko, A., *et al.* (2021). Highly accurate protein structure prediction with AlphaFold. *Nature*, 596(7873), 583–589.
- [2] Yang, Z., Zeng, X., Zhao, Y., & Chen, R. (2023). AlphaFold2 and its applications in the fields of biology and medicine. *Signal Transduction and Targeted Therapy*, 8(1), 115.
- [3] Cramer, P. (2021). AlphaFold2 and the future of structural biology. *Nature Structural & Molecular Biology*, 28(9), 704–705.
- [4] Akdel, M., Pires, D. E. V., Porta Pardo, E., Jänes, J., Zalevsky, A. O., Mészáros, B., Bryant, P., Good, L. L., Laskowski, R. A., Pozzati, G., *et al.* (2022). A structural biology community assessment of AlphaFold2 applications. *Nature Structural & Molecular Biology*, 29(11), 1056–1067.
- [5] Peng, X., Luo, S., Guan, J., Xie, Q., Peng, J., & Ma, J. (2022). Pocket2Mol: Efficient molecular sampling based on 3-D protein pockets. *Proceedings of the 39th International Conference on Machine Learning (ICML)*, 17644–17655.
- [6] Jiang, Y., Zhang, G., You, J., Zhang, H., Yao, R., Xie, H., Zhang, L., Xia, Z., Dai, M., Wu, Y., *et al.* (2024). PocketFlow is a data- and knowledge-driven structure-based molecular generative model. *Nature Machine Intelligence*, 6(3), 326–337.
- [7] Feng, W., Wang, L., Lin, Z., Zhu, Y., Wang, H., Dong, J., Bai, R., Wang, H., Zhou, J., Peng, W., *et al.* (2024). Generation of 3-D molecules in pockets via a language model. *Nature Machine Intelligence*, 6(1), 62–73.
- [8] Liu, M., Luo, Y., Uchino, K., Maruhashi, K., & Ji, S. (2022). Generating 3-D molecules for target protein binding. *arXiv preprint arXiv:2204.09410*.
- [9] Lin, H., Zhao, G., Zhang, O., Huang, Y., Wu, L., Liu, Z., Li, S., Tan, C., Gao, Z., & Li, S. Z. (2024). CBGBench: Fill in the blank of protein-molecule complex binding graph. *arXiv preprint arXiv:2406.10840*.
- [10] Zhang, O., Zhang, J., Jin, J., Zhang, X., Hu, R., Shen, C., Cao, H., Du, H., Kang, Y., Deng, Y., *et al.* (2023). ResGen is a pocket-aware 3-D molecular generation model based on parallel multiscale modelling. *Nature Machine Intelligence*, 5(9), 1020–1030.
- [11] Zhang, O., Huang, Y., Cheng, S., Yu, M., Zhang, X., Lin, H., Zeng, Y., Wang, M., Wu, Z., & Zhao, H. (2024). FragGen: Towards 3-D geometry-reliable fragment-based molecular generation. *Chemical Science*, 15(46), 19452–19465.
- [12] Ho, J., Jain, A., & Abbeel, P. (2020). Denoising diffusion probabilistic models. *Advances in Neural Information Processing Systems*, 33, 6840–6851.
- [13] Nichol, A. Q., & Dhariwal, P. (2021). Improved denoising diffusion probabilistic models. *Proceedings of the 38th International Conference on Machine Learning (ICML)*, 8162–8171.

- [14] Song, J., Meng, C., & Ermon, S. (2020). Denoising diffusion implicit models. arXiv preprint arXiv:2010.02502.
- [15] Song, Y., Sohl-Dickstein, J., Kingma, D. P., Kumar, A., Ermon, S., & Poole, B. (2020). Score-based generative modeling through stochastic differential equations. arXiv preprint arXiv:2011.13456.
- [16] Vahdat, A., Kreis, K., & Kautz, J. (2021). Score-based generative modeling in latent space. *Advances in Neural Information Processing Systems*, 34, 11287–11302.
- [17] Song, Y., & Ermon, S. (2020). Improved techniques for training score-based generative models. *Advances in Neural Information Processing Systems*, 33, 12438–12448.
- [18] Hoogeboom, E., Garcia Satorras, V., Vignac, C., & Welling, M. (2022). Equivariant diffusion for molecule generation in 3-D. *Proceedings of the 39th International Conference on Machine Learning (ICML)*, 8867–8887.
- [19] Cornet, F., Bartosh, G., Schmidt, M., & Naesseth, C. A. (2024). Equivariant neural diffusion for molecule generation. *Advances in Neural Information Processing Systems*, 37, 49429–49460.
- [20] Schneuing, A., Harris, C., Du, Y., Didi, K., Jamsab, A., Igashov, I., Du, W., Gomes, C., Blundell, T. L., & Liò, P., *et al.* (2024). Structure-based drug design with equivariant diffusion models. *Nature Computational Science*, 4(12), 899–909.
- [21] Gu, S., Xu, M., Powers, A., Nie, W., Geffner, T., Kreis, K., Leskovec, J., Vahdat, A., & Ermon, S. (2024). Aligning target-aware molecule diffusion models with exact energy optimization. *Advances in Neural Information Processing Systems*, 37, 44040–44063.
- [22] Guan, J., Qian, W. W., Peng, X., Su, Y., Peng, J., & Ma, J. (2023). 3-D equivariant diffusion for target-aware molecule generation and affinity prediction. arXiv preprint arXiv:2303.03543.
- [23] Qian, H., Huang, W., Tu, S., & Xu, L. (2024). KGDiff: Towards explainable target-aware molecule generation with knowledge guidance. *Briefings in Bioinformatics*, 25(1), bbad435.
- [24] Guan, J., Zhou, X., Yang, Y., Bao, Y., Peng, J., Ma, J., Liu, Q., Wang, L., & Gu, Q. (2024). DecompDiff: Diffusion models with decomposed priors for structure-based drug design. arXiv preprint arXiv:2403.07902.
- [25] Xu, M., Powers, A., Dror, R., Ermon, S., & Leskovec, J. (2023). Geometric latent diffusion models for 3-D molecule generation. *Proceedings of the 40th International Conference on Machine Learning (ICML)*, 38592–38610.
- [26] Lin, H., Huang, Y., Zhang, O., Ma, S., Liu, M., Li, X., Wu, L., Wang, J., Hou, T., & Li, S. Z. (2025). DiffBP: Generative diffusion of 3-D molecules for target protein binding. *Chemical Science*, 16(3), 1417–1431.
- [27] Lin, H., Huang, Y., Zhang, O., Liu, Y., Wu, L., Li, S., Chen, Z., & Li, S. Z. (2023). Functional-group-based diffusion for pocket-specific molecule generation and elaboration. *Advances in Neural Information Processing Systems*, 36, 34603–34626.
- [28] Zhang, Z., Min, Y., Zheng, S., & Liu, Q. (2023). Molecule generation for target protein binding with structural motifs. *Proceedings of the 11th International Conference on Learning Representations (ICLR)*.
- [29] Kong, X., Zhang, Z., Zhang, Z., Jiao, R., Ma, J., Liu, K., & Huang, W., *et al.* (2025). UniMoMo: Unified generative modeling of 3-D molecules for de novo binder design. arXiv preprint arXiv:2503.19300.
- [30] Halgren, T. A. (1999). MMFF VI. MMFF94s option for energy minimization studies. *Journal of Computational Chemistry*, 20(7), 720–729.
- [31] Irwin, J. J., Tang, K. G., Young, J., Dandarchuluun, C., Wong, B., Khurelbaatar, M., Moroz, Y., Mayfield, J., & Sayle, R. A. (2020). ZINC20—A free ultralarge-scale chemical database for ligand discovery. *Journal of Chemical Information and Modeling*, 60(12), 6065–6073.

- [32] Zhang, Y., & Skolnick, J. (2005). TM-align: A protein structure alignment algorithm based on the TM-score. *Nucleic Acids Research*, 33(7), 2302–2309.
- [33] Holm, L., & Park, J. (2000). DaliLite workbench for protein structure comparison. *Bioinformatics*, 16(6), 566–567.
- [34] Zhang, Z., & Liu, Q. (2023). Learning subpocket prototypes for generalizable structure-based drug design. *Proceedings of the 40th International Conference on Machine Learning (ICML)*, 41382–41398.
- [35] Notarangelo, L. D., Kim, M. S., Walter, J. E., & Lee, Y. N. (2016). Human RAG mutations: Biochemistry and clinical implications. *Nature Reviews Immunology*, 16(4), 234–246.
- [36] Edge, D., Trinh, H., Cheng, N., Bradley, J., Chao, A., Mody, A., Truitt, S., Metropolitansky, D., Ness, R. O., & Larson, J. (2024). From local to global: A graph RAG approach to query-focused summarization. *arXiv preprint arXiv:2404.16130*.
- [37] Toro, S., Anagnostopoulos, A. V., Bello, S., Blumberg, K., Cameron, R., Carmody, L., *et al.* (2024). Dynamic retrieval-augmented generation of ontologies using artificial intelligence (DRAGON-AI). *Journal of Biomedical Semantics*, 15(1), 19.
- [38] Imrie, F., Bradley, A. R., van der Schaar, M., & Deane, C. M. (2020). Deep generative models for 3-D linker design. *Journal of Chemical Information and Modeling*, 60(4), 1983–1995.
- [39] Lee, S., Kreis, K., Veccham, S., Liu, M., Reidenbach, D., Paliwal, S., & Nie, W. (2024). Molecule generation with fragment retrieval augmentation. *Advances in Neural Information Processing Systems*, 37, 132463–132490.
- [40] Wang, H., Li, W., Jin, X., Cho, K., Ji, H., & Han, J., & Burke, M. D. (2021). Chemical-reaction-aware molecule representation learning. *arXiv preprint arXiv:2109.09888*.
- [41] Huang, L., Xu, T., Yu, Y., Zhao, P., Chen, X., Han, J., Xie, Z., Li, H., Zhong, W., Wong, K. C., *et al.* (2024). A dual diffusion model enables 3-D molecule generation and lead optimization based on target pockets. *Nature Communications*, 15(1), 2657.
- [42] Liu, L., He, D., Fang, X., Zhang, S., Wang, F., He, J., & Wu, H. (2022). GEM-2: Next-generation molecular property prediction network by modeling full-range many-body interactions. *arXiv preprint arXiv:2208.05863*.
- [43] Wang, Y., Wang, J., Cao, Z., & Farimani, A. B. (2022). Molecular contrastive learning of representations via graph neural networks. *Nature Machine Intelligence*, 4(3), 279–287.
- [44] Liu, Z., Yang, D., Wang, Y., Lu, M., & Li, R. (2023). EGNN: Graph structure learning based on evolutionary computation helps more in graph neural networks. *Applied Soft Computing*, 135, 110040.
- [45] Yu, S., Kwak, S., Jang, H., Jeong, J., Huang, J., & Shin, J., & Xie, S. (2024). Representation alignment for generation: Training diffusion transformers is easier than you think. *arXiv preprint arXiv:2410.06940*.
- [46] Bodenhofer, U., Bonatesta, E., Horejš-Kainrath, C., & Hochreiter, S. (2015). msa: An R package for multiple sequence alignment. *Bioinformatics*, 31(24), 3997–3999.
- [47] Trott, O., & Olson, A. J. (2010). AutoDock Vina: Improving the speed and accuracy of docking with a new scoring function, efficient optimization, and multithreading. *Journal of Computational Chemistry*, 31(2), 455–461.
- [48] Masuda, T., Ragoza, M., & Koes, D. R. (2020). Generating 3-D molecular structures conditional on a receptor binding site with deep generative models. *arXiv preprint arXiv:2010.14442*.
- [49] Luo, S., Guan, J., Ma, J., & Peng, J. (2021). A 3-D generative model for structure-based drug design. *Advances in Neural Information Processing Systems*, 34, 6229–6239.
- [50] Qu, Y., Qiu, K., Song, Y., Gong, J., Han, J., Zheng, M., & Zhou, H., & Ma, W. (2024). MolCraft: Structure-based drug design in continuous parameter space. *arXiv preprint arXiv:2404.12141*.

- [51] Pinheiro, P. O., Jamasb, A., Mahmood, O., Sresht, V., & Saremi, S. (2024). Structure-based drug design by denoising voxel grids. arXiv preprint arXiv:2405.03961.
- [52] Salentin, S., Schreiber, S., Haupt, V. J., Adasme, M. F., & Schroeder, M. (2015). PLIP: Fully automated protein–ligand interaction profiler. *Nucleic Acids Research*, 43(W1), W443–W447.
- [53] Wang, Z., Nie, W., Qiao, Z., Xiao, C., Baraniuk, R., & Anandkumar, A. (2022). Retrieval-based controllable molecule generation. arXiv preprint arXiv:2208.11126.